# Spectroscopic and Electronic Structural Studies of Blue Copper Model Complexes. 1. Perturbation of the Thiolate−Cu Bond

**David W. Randall,[†] Serena DeBeer George,[†] Britt Hedman,[†,‡] Keith O. Hodgson,[†,‡] Kiyoshi Fujisawa,*[,§] and Edward I. Solomon*[,†]**

*Contribution from the Department of Chemistry, Stanford University, 333 Campus Drive, Stanford, California 94305, Stanford Synchrotron Radiation Laboratory, Stanford Linear Accelerator Center, Stanford University, Stanford, California 94309, and Department of Chemistry, University of Tsukuba, Tsukuba 305-8571 Japan*

*Received May 9, 2000. Revised Manuscript Received August 30, 2000*

**Abstract:** A tris(pyrazolyl)hydroborate triphenylmethylthiolate Cu(II) model complex (**1**) that reproduces structural and spectroscopic features of active sites of blue Cu proteins is characterized using low-temperature absorption, magnetic circular dichroism (MCD), X-ray absorption (XAS), and resonance Raman (rR) spectroscopies combined with DFT calculations to define its electronic structure. The electronic structure of **1** is further related to the oxidized Cu site in plastocyanin. The key spectral differences relative to plastocyanin include an increase in the intensity of the S p$\pi$ → Cu CT band and a decrease in the absorption intensity at ∼450 nm. The energies of d → d transitions in **1** decrease relative to plastocyanin, which reflects the more tetrahedral geometry of **1**. S K-edge XAS measurements demonstrate a more covalent thiolate interaction in the HOMO of **1** (52% S p) than in plastocyanin (38% S p). The effects of the high thiolate covalency on the absorption and Raman spectral features for **1** are evaluated. Additional changes in the absorption spectrum of **1** relative to plastocyanin in the ∼450 nm and the near-infrared regions are due to differences in the electronic structure of the nitrogen ligands associated with the change from imidazole to pyrazole. Finally, XAS measurements at the Cu L- and K-edges indicate that the effective nuclear charge of Cu in **1** is higher than in plastocyanin, which likely results from misdirection of the ligating orbitals in the constrained tris(pyrazolyl)-hydroborate ligand system. This reduces the donor interaction of this ligand with the copper which increases the covalency of the thiolate−Cu bond and can contribute to the electron-transfer properties of the blue copper site.

## 1. Introduction

Blue (or Type 1) Cu centers in proteins are critical components of biological electron transfer (ET) pathways in a diverse range of organisms. These metalloproteins are involved in intra- and interprotein biological ET processes of global importance, including photosynthesis, nitrogen fixation, and lignin degradation.[1−5] The prototypical blue Cu center in the protein plastocyanin has been structurally characterized.[6,7] Figure 1A presents the structure of the active site of this protein, the geometry of which is best described as approximately trigonally distorted tetrahedral. The three equatorial ligands include two normal 2.0 Å Cu−N(His) bonds and an unusually short 2.1 Å Cu−S(Cys) thiolate bond. The axial ligand is an S(Met) with an unusually long Cu−S(Met) distance of ∼2.8 Å.[7] These unique structural features impart the site with unique spectral features, the most obvious being the intense, low-energy charge-transfer (CT) band at 600 nm, which is responsible for the blue color of these proteins. In the EPR spectrum, the Cu hyperfine interaction is reduced relative to that of normal tetragonal Cu centers. In plastocyanin, these spectral features result from a very covalent Cu−S(Cys) interaction.[8]

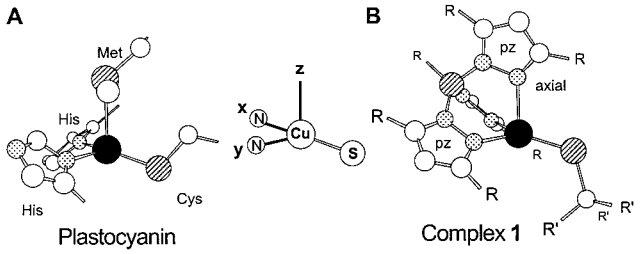


**Figure 1.** Copper thiolate centers: (A) plastocyanin and (B) tris-(pyrazolyl)hydroborate triphenylmethylthiolate copper, complex **1**; R = isopropyl, R′ = phenyl.

Although these proteins have been the subject of extensive study, model complexes of the oxidized protein have proven generally elusive due to synthetic obstacles.[9,10] The unusual

* To whom correspondence should be addressed. E-mail: Fax: (650) 725-0259. Edward.Solomon@stanford.edu.
[†] Department of Chemistry, Stanford University.
[‡] Stanford Synchrotron Radiation Laboratory, Stanford Linear Accelerator Center, Stanford University.
[§] University of Tsukuba.

(1) Messerschmidt, A. *Struct. Bonding* **1998**, *90*, 37−68.
(2) Sykes, A. G. *Struct. Bonding* **1991**, *75*, 175−224.
(3) Adman, E. T. *Adv. Protein Chem.* **1991**, *42*, 145−197.
(4) Gray, H. B.; Solomon, E. I. In *Copper Proteins*; Spiro, T. G., Ed.; Wiley: New York, 1981; pp 1−39.
(5) Solomon, E. I.; Lowery, M. D.; Guckert, J. A.; LaCroix, L. B. *Adv. Chem. Ser.* **1997**, *253*, 317−330.
(6) Colman, P. M.; Freeman, H. C.; Guss, J. M.; Murata, M.; Norris, V. A.; Ramshaw, J. A. M.; Venkatappa, M. P. *Nature* **1978**, *272*, 319−324.
(7) Guss, J. M.; Bartunik, H. D.; Freeman, H. C. *Acta Crystallogr.* **1992**, *B48*, 790−811.
(8) Solomon, E. I.; Penfield, K. W.; Gewirth, A. A.; Lowery, M. D.; Shadle, S. E.; Guckert, J. A.; LaCroix, L. B. *Inorg. Chim. Acta* **1996**, *243*, 67−78.

10.1021/ja001591w CCC: $19.00 
Published on Web 11/08/2000

trigonally distorted tetrahedral geometry of the oxidized blue Cu centers presents an additional synthetic challenge because it is so different from the tetragonally distorted geometry typically observed for Cu(II). By utilizing the rigid framework afforded by the tridentate tris(pyrazolyl)hydroborate [$HB(pz')_3^-$] ligand system and by choosing an appropriate solvent system, Kitajima, Fujisawa, and Moro-oka prepared[11,12] the trigonally distorted tetrahedral complex (**1**, Figure 1B) that mimics many spectroscopic and metric features of the blue Cu active site, including the strong absorption at ∼600 nm, the small Cu $A_{||}$ hyperfine interaction in the EPR, and the short Cu−S(thiolate) distance of 2.1 Å.[10−12] The two Cu−N(pz) distances in the equatorial plane are typical at ∼2.0 Å, while the axial Cu−N(pz) distance is somewhat longer at 2.2 Å. The triphenylmethylthiolate completes the equatorial ligation sphere. The structure of complex **1** differs from that found in prototypical blue Cu proteins[7] in two respects: the thiolate ligand has changed from cysteinate to triphenylmethylthiolate, while the $N(His)_2S(Met)$ donor sphere has been replaced by tridentate [$HB(pz')_3^-$].

In this mulitfaceted spectroscopic study of $LCuSCPh_3$ [**1**, L = tris(3,5-diisopropylpyrazolyl)hydroborate], differences in the electronic structures between the synthetic complex and plastocyanin are investigated. Spectroscopic techniques including low-temperature absorption, low-temperature magnetic circular dichroism (MCD), resonance Raman enhancement profile (RREP) analysis, and X-ray absorption spectroscopy (XAS) are complemented by density functional calculations and are applied to define the electronic structure of this model complex. A comparison of the spectroscopic features of **1** to those previously defined for the prototypical blue Cu site in plastocyanin allows us to probe the differences in the electronic structures of the protein site and this synthetic model system. In particular, this study examines the effects on the geometric and electronic structure resulting from variation in the nature of the thiolate ligand relative to that in the protein (i.e., triphenylmethylthiolate vs cysteinate) as well as the nature of the equatorial nitrogen ligand donor set (i.e., pyrazole vs imidazole).

## 2. Experimental Procedures

**2.1. Compounds.** The $HB(pz')_3$Cu(II)thiolate complex **1** was synthesized as described elsewhere.[10−12] A preliminary X-ray crystal structure of **1** has been reported.[12,13] For the present study, a crystal structure of higher quality was obtained. The following are available in the Supporting Information: specific details for crystal structure determination, atomic numbering of **1**·($C_7H_{16}$), tables listing positional and isotropic thermal parameters, anisotropic thermal parameters, bond lengths and angles, and torsion angles.

**2.2. UV−Vis Absorption and MCD Spectroscopy.** Low-temperature UV−vis absorption spectra were recorded at ∼10 K on a Cary 17 equipped with a Janis Supervaritemp dewar. MCD spectra were recorded using Jasco J500 (UV−vis, PMT detection) and Jasco J200 (near-IR, liquid nitrogen cooled InSb solid-state detection) spectropolarimeters modified to include Oxford SM-4 (7 T, UV−vis) or SM-4000 (7 T, near-IR) superconducting magnets with optical access within their sample compartments. Special care was taken to provide magnetic shielding for the PMT detector. Solid samples (mulls) for spectroscopy that were prepared by finely grinding microcrystalline material into powders with a mortar and pestle and then adding mulling agents (poly(dimethylsiloxane) (Aldrich) or Fluorolube (Wilmad)) were uniformly spread between quartz disks (Heraeus-Amersil) and loaded into copper MCD cells and promptly frozen.

**2.3. Raman Enhancement Profiles.** Raman spectra were recorded using a Princeton Instruments, liquid nitrogen cooled, back illuminated CCD camera mounted on a Spex 1877 0.6 m triple spectrometer, equipped with holographic gratings blazed at 1200, 1800, or 2400 grooves/mm. Continuous wave Coherent Kr ion (Innova 90C-K) and Ar ion (Sabre-25/7) visible and UV laser lines were used as variable energy excitation sources. A polarization scrambler was placed in front of the entrance slits of the spectrometer. Samples were loaded in 5-mm (o.d.) NMR tubes and stored in liquid nitrogen. Spectra were obtained in a ∼135° backscattering geometry with ∼40 mW incident power. Raman scattering resolution and accuracy are ∼2 $cm^{-1}$. Raman peak profile intensities were determined relative to solvent peaks or in the case of solid samples relative to the 995 $cm^{-1}$ band of $Na_2SO_4$. Resonance Raman enhancement profiles (RREPs) were simulated using the time-dependent theory of Heller, et al.[14−18] that was implemented in a MathCAD script.[19] The parameters of the fits were adjusted until the simulated spectra reasonably matched the experimental data. The same set of parameters was used to simulate both the resonance Raman enhancement profile and the absorption spectrum.

**2.4. X-ray Absorption Spectroscopy Measurements and Data Analysis.** All data were measured at the Stanford Synchrotron Radiation Laboratory under ring conditions 3.0 GeV and 60−100 mA.

S K-edge data were measured using the 54-pole wiggler beam line 6-2 in high magnetic field mode of 10 kG with a Ni-coated harmonic rejection mirror and fully tuned Si(111) double crystal monochromator. Details of the optimization of this setup for low-energy studies have been described in an earlier publication.[20] S K-edge measurements were made at room temperature. Samples were ground into a fine powder and dispersed as thinly as possible on Mylar tape to minimize the possibility of self-absorption. The data were measured as fluorescence excitation spectra utilizing an ionization chamber as a fluorescence detector.[21,22] To check for reproducibility, 2−3 scans were measured for each solid sample. The energy was calibrated from S K-edge spectra of $Na_2S_2O_3$·$5H_2O$, run at intervals between sample scans. The maximum of the first preedge feature in its spectrum was assigned to 2472.02 eV. Data were averaged, and a smooth background was removed from all spectra by fitting a polynomial to the preedge region and subtracting this polynomial from the entire spectrum. Normalization of the data was accomplished by fitting a flattened polynomial or straight line to the postedge region and normalizing the edge jump to 1.0 at 2490 eV. Fits to the edges were performed using the program EDG_FIT.[23] Second derivative spectra were used as guides to determine the number and position of peaks. Preedge and rising edge features were modeled by pseudo-Voigt line shapes. For the preedge feature, a fixed 1:1 ratio of Lorentzian to Gaussian contributions was used. Fits were performed over several energy ranges. The reported intensity values are based on the average of all good fits. Normalization procedures can introduce ∼3% error in preedge peak intensities, in addition to the error resulting from the fitting procedure.

Cu L-edge data were measured using the 31-pole wiggler beam line 10-1. Samples were finely ground and spread across double-adhesive

(9) Mandal, S.; Das, G.; Singh, R.; Shukla, R.; Bharadwaj, P. K. *Coord. Chem. Rev.* **1997**, *160*, 191−235.
(10) Kitajima, N. *Adv. Inorg. Chem.* **1992**, *39*, 1−77.
(11) Kitajima, N.; Fujisawa, K.; Moro-oka, Y. *J. Am. Chem. Soc.* **1990**, *112*, 3210−3212.
(12) Kitajima, N.; Fujisawa, K.; Tanaka, M.; Moro-oka, Y. *J. Am. Chem. Soc.* **1992**, *114*, 9232−9233.
(13) Qiu, D.; Kilpatrick, L. T.; Kitajima, N.; Spiro, T. G. *J. Am. Chem. Soc.* **1994**, *116*, 2585−2590.
(14) Heller, E. J. *Acc. Chem. Res.* **1981**, *14*, 368−375.
(15) Heller, E. J.; Sundberg, R. L.; Tannor, D. *J. Phys. Chem.* **1982**, *86*, 1822−1833.
(16) Myers, A. B.; Mathies, R. A. In *Biological Applications of Raman Spectroscopy*; Spiro, T. G., Ed.; Wiley: New York, 1987; Vol. 2, pp 1−58.
(17) Myers, A. B. *Acc. Chem. Res.* **1997**, *30*, 519−527.
(18) Zink, J. I.; Shin, K. S. K. *Adv. Photochem.* **1991**, *16*, 119−214.
(19) Brunold, T. C.; Tamura, N.; Kitajima, N.; Moro-oka, Y.; Solomon, E. I. *J. Am. Chem. Soc.* **1998**, *120*, 5674−5690.
(20) Hedman, B.; Frank, P.; Gheller, S. F.; Roe, A. L.; Newton, W. E.; Hodgson, K. O. *J. Am. Chem. Soc.* **1988**, *110*, 3798−3805.
(21) Stern, E. A.; Heald, S. M. *Rev. Sci. Instrum.* **1979**, *50*, 1579−1582.
(22) Lytle, F. W.; Greegor, R. B.; Sandstrom, D. R.; Marques, E. C.; Wong, J.; Spiro, C. L.; Huffman, G. P.; Huggins, F. E. *Nucl. Instrum. Methods* **1984**, *226*, 542−548.
(23) George, G. N. EDG_FIT; Stanford Synchrotron Radiation Laboratory, Stanford Linear Accelerator Center, Stanford University, Stanford, CA 94309.

conductive carbon tape, which was attached to an aluminum paddle. The data were measured at room temperature as total electron yield spectra utilizing a Galileo 4716 channeltron electron multiplier as a detector. For each sample, 3−4 scans were measured to check reproducibility. The energy was calibrated from the Cu L-edge spectra of $CuF_2$, run at intervals between sample scans. The maximum of the $L_3$ and $L_2$ preedges were assigned to 930.5 and 950.5 eV, respectively. A linear background was fit to the preedge region (870−920 eV) and was subtracted from the entire spectrum. Normalization was accomplished by fitting a straight line to the postedge region and normalizing the edge jump to 1.0 at 1000 eV. Fits to the edges were performed using EDG_FIT.[23] A pseudo-Voigt peak was used to model the $L_3$ and $L_2$ 2p → 3d transitions. Arctangent functions were used to model the $L_3$ and $L_2$ edge jumps. The total L-preedge intensity reported here was calculated as $L_3 + L_2$. The reported intensity values are based on the average of all good fits. Normalization procedures can introduce ∼4% error in preedge peak intensities, in addition to the error resulting from the fitting procedure.

Cu K-edge XAS data were measured using the unfocused 8-pole wiggler beam line 7−3 and utilized a Si(220) monochromator for energy selection at the Cu K-edge. The monochromator was detuned 50% to minimize higher harmonic components in the X-ray beam. Samples for Cu K-edge XAS studies were prepared as solids in boron nitride. The mixture was pressed into a pellet and sealed between 63.5-$\mu$m Mylar tape windows in a 1-mm aluminum spacer. The samples were immediately frozen and stored in liquid nitrogen and were maintained at 10 K during data collection using an Oxford Instruments CF1208 continuous flow liquid helium cryostat. Data were measured in transmission mode to $k = 15$ Å$^{-1}$. Internal energy calibration was performed by simultaneous measurement of the absorption of a Cu foil placed between a second and third ionization chamber. The first inflection point was assigned to 8980.3 eV. The data represent a three-scan average and were processed by fitting a second-order polynomial to the postedge region and subtracting this background from the entire spectrum.[24] A three-region cubic spline was used to model the smooth background above the edge. The data were normalized by subtracting the spline and normalizing the edge jump to 1.0 at 9000 eV.

**2.5 Calculations.** Density functional theory (DFT) calculations were performed using the Amsterdam Density Functional package of Baerends and co-workers (ADF2.0.1) using the database IV basis set.[25,26] The Vosko, Wilk, Nusair local density approximation[27] was used for exchange and correlation. Generalized gradient approximations of Becke[28] and Perdew[29] were included for exchange and correlation. The calculations reported here are for spin-restricted systems; however, spin-unrestricted calculations gave very similar results. To model the geometry of **1**, the entire $[HB(pz)_3^-]$ ligand was retained. The calculations reported here model the thiolate as $SCH_3^-$; however calculations where the entire triphenylmethylthiolate was included did not substantially alter the results. The resulting $[HB(pz)_3]CuSCH_3$ complex was based on the crystal structure, giving a complex with $C_1$ symmetry. Input files, including the atomic coordinates, are included in the Supporting Information.

## 3. Results and Analysis

### 3.1. Absorption and Magnetic Circular Dichroism.

**3.1.1. Absorption.** From the low-temperature mull spectrum in Figure 2A, the absorption spectrum of **1** is dominated by an intense transition at 625 nm (16000 cm$^{-1}$), band 6. The features observed in this spectrum closely match those that have been previously reported for this compound in solution.[10,12] To lower energy, bands 4 and 5 occur at 10820 and 11080 cm$^{-1}$, respectively. Band 4 ($\epsilon \approx 990$ M$^{-1}$ cm$^{-1}$) is more intense than band 5 ($\epsilon \approx 520$ M$^{-1}$ cm$^{-1}$). No obvious absorption features associated with **1** appear to lower energy than 10000 cm$^{-1}$. Very weak transitions occur at 20400 cm$^{-1}$ (band 8) and 23300 cm$^{-1}$ (band 9). A weak absorption feature is observed at 28500 cm$^{-1}$ (marked with an *), which is due to a small amount of an impurity in the sample.[10,30] Table 1 summarizes the Gaussians that simultaneously fit both the absorption and MCD spectra (vide infra) and are included in Figure 2A.

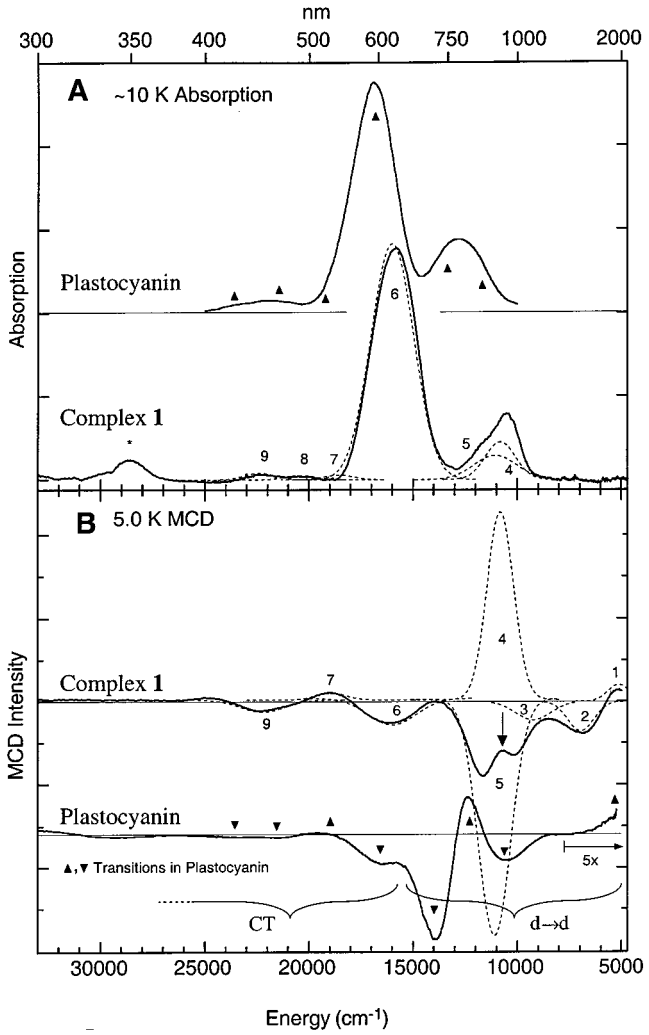


**Figure 2.** Excited-state electronic spectra of complex **1** in comparison to plastocyanin.[32] (A) 10 K absorption spectrum of **1** (mull), including an overlay of Gaussian fits summarized in Table 1. (B) Low temperature (5 K) magnetic circular dichroism (MCD) spectrum of **1** (mull) at a field of 7 T, including Gaussian fits summarized in Table 1. For plastocyanin, the band positions (closed triangles) are indicated in both panels as are the CT and d → d regions in panel B.

**3.1.2 Magnetic Circular Dichroism.** The MCD technique is a powerful complement to absorption studies of paramagnetic species such as **1**, because MCD transitions gain intensity through a mechanism that selectively enhances the d → d transitions that are often weak in absorption. The MCD transitions also have a sign, which can facilitate resolution. The low temperature (5.0 K) mull MCD spectrum is presented in Figure 2B. Gaussian fits to the peaks are also included in Figure 2B and summarized in Table 1. In the lowest-energy region (5000−12000 cm$^{-1}$) in Figure 2B are the most intense features

(24) DeWitt, J. G.; Bentsen, J. G.; Rosenzweig, A. C.; Hedman, B.; Green, J.; Pilkington, S.; Papaefthymiou, G. C.; Dalton, H.; Hodgson, K. O.; Lippard, S. J. *J. Am. Chem. Soc.* **1991**, *113*, 9219−9235.
(25) ADF 2.0.1; Vrije Universiteit, Theoretical Chemistry, De Boelelaan 1083, 1081 HV Amsterdam, The Netherlands, 1995.
(26) te Velde, G.; Baerends, E. J. *J. Comput. Phys.* **1992**, *99*, 84−98.
(27) Vosko, S. H.; Wilk, L.; Nusair, M. *Can. J. Phys.* **1980**, *58*, 1200−1211.
(28) Becke, A. D. *Phys. Rev. A* **1988**, *38*, 3098−3100.
(29) Perdew, J. P. *Phys. Rev. B* **1986**, *33*, 8822−8224.
(30) Fujisawa, K.; Moro-oka, Y.; Kitajima, N. *J. Chem. Soc., Chem. Commun.* **1995**, 623−624.

**Table 1.** Experimental MCD and Absorption Band Characterization for **1**

| band | assignment | energy ($cm^{-1}$) | $\epsilon$ ($M^{-1}$ $cm^{-1}$)[a] | osc str[a] | MCD/ABS[b] |
|---|---|---|---|---|---|
| 1 | $d_{z^2}$ | 5200 | − | nd | +ve |
| 2 | pz | ∼7000 | − | nd | −ve |
| 3 | $d_{xy}$ | 9250 | − | nd | −ve |
| 4 | $d_{yz+xz}$ | 10820 | 990 | 0.0090 | +0.490 |
| 5 | $d_{yz-xz}$ | 11080 | 520 | 0.0033 | −1.000 |
| 6 | S p$\pi$ CT | 16000 | 6340 | 0.0713 | −0.012 |
| 7 | S p ps.$\sigma$ | 18650 | ∼40 | 0.0002 | +ve |
| 8 | pz | 20400 | − | nd | nd |
| 9 | pz | 23300 | 60 | 0.0005 | −ve |

[a] Based on −45 °C absorption spectrum. [b] Normalized ratio of MCD intensity to absorption intensity. This ratio approximates the relative *C*/*D* ratios for mull data, where it is not possible to obtain absolute *C*/*D* ratios.

of the MCD spectrum. In analogy to plastocyanin, whose spectra are included in Figure 2 for reference, and similar Cu(II)−thiolate centers,[31,32] the two highest-energy d → d transitions are expected to exhibit a "pseudo-A" pattern[33] that is due to spin−orbit coupling between the two excited states. This situation imparts opposite *C*-term[33] signs to two MCD transitions that are close in energy.[34] Evidence of such a pattern in the MCD spectrum of **1** is observed at 11000 $cm^{-1}$ in the feature marked in Figure 2B with an arrow. For this feature to be a pseudo-A spectral pattern, an additional negatively overlapping band (band 3) must be included in the fits. Including band 3 permits bands 4 and 5 to have similar widths as expected and observed for plastocyanin.[31,32] Band 6 at 16000 $cm^{-1}$, which is relatively weak in the MCD spectrum, corresponds to the strong 625 nm absorption feature. To higher energy are bands 7 and 9, which are even less intense. The temperature dependence of the MCD spectral intensity indicates that all bands are due also to a *C*-term mechanism. The saturation behavior of the MCD features indicates a $g_{iso}$ value of 2.17 that is consistent with the value measured by EPR ($g_{iso}$(EPR) ≈ 2.12),[10,11] although EPR more precisely resolves the anisotropy in the electronic Zeeman interaction.

**3.1.3. Band Assignments.** The bands observed in the absorption and MCD spectra of **1** can be classified as ligand field or charge transfer (CT) from the intensities in the MCD spectrum relative to the absorption spectrum. The $\sim C_s$ symmetry of the Cu site in **1** precludes orbital degeneracy and all MCD *C*-term intensity must derive from mixing of orthogonal transition moments that result from out-of-state spin−orbit coupling (SOC).[31] The ratio of the MCD intensity to the absorption intensity, that is, MCD/ABS, which approximates the $C_0/D_0$ ratio[33] for a mull, will depend on the magnitude of the SOC between states, which scales with the SOC constant, $\xi$. Accordingly, the significant Cu character of the d → d transitions imparts them with substantial MCD intensity since Cu has a $\xi$ value (830 $cm^{-1}$) that is considerably larger than that of S (380 $cm^{-1}$) or N (70 $cm^{-1}$). States which are close in energy and have orthogonal transition moments can spin−orbit couple to form a pseudo-A signal that is composed of oppositely signed C-term transitions. However, if the energy separation is not large, the intensities of the individual transitions mostly cancel, which appears to be the case for bands 4 and 5 in Figure 2B. Overlap of the positive intensity of band 4 with another negative band (band 3) further obscures the pseudo-A feature. Therefore, four of the most intense, low-energy bands in the MCD spectrum (bands 1, 3−5) can be classified as d → d bands. Band 2 does not have a counterpart in plastocyanin and appears to be associated with the tris(pyrazole)hydroborate ligand (vide infra).

For **1**, the smaller MCD/ABS ($\sim C_0/D_0$) ratio of the intense band at 16000 $cm^{-1}$ (band 6) and resonance Raman enhancement profile (RREP, vide infra) data clearly indicate that this transition is the S(thiolate) → HOMO charge-transfer (CT) transition. Based on the low energy of this CT transition that lies just above the LF (ligand field) block and its negative MCD sign, the intense 625 nm absorption band is assigned as the S p$\pi$ → Cu CT transition. This assignment parallels the assignment for this band in blue Cu centers, such as plastocyanin.[31,32] To immediately higher energy of this transition lies band 7 at 18650 $cm^{-1}$, which is relatively weak. The MCD sign of this band is positive, which is the same sign as observed for the S p pseudo-$\sigma$ → HOMO CT transition in blue Cu proteins.[31,32,35,36] Band 7 in **1** is therefore assigned as this transition. To higher energy, bands 8 and 9 are likely N(pyrazole) → HOMO transitions, since they have observable MCD intensity, which implies some Cu character.

The specific assignments of the individual LF bands in **1** follow those in plastocyanin (the coordinate system is given in Figure 1, where *z* is perpendicular to the S(thiolate)$N_2$ plane and *x* and *y* are bisected by the S(thiolate)−Cu bond). Following the argument in ref 32, the absorption intensity of the two highest energy LF bands derives from configuration interaction mixing with the more intense S → Cu CT transitions to higher energy. The $d_{yz+xz}$ orbital has the correct symmetry to interact with the S p$\pi$ orbital, while the $d_{yx-xz}$ orbital has the correct symmetry to interact with the S pseudo-$\sigma$ orbital. The increased intensity of band 4 relative to band 5 in the absorption spectrum indicates that band 4 is the $d_{yz+xz}$ → HOMO transition, while band 5 at higher energy is the $d_{yz-xz}$ → HOMO transition. On the basis of trends in the $g_{||}$ values and the energies of the two lowest-lying d → d transitions in many blue Cu proteins[36] the following assignments can be made for these two d → d bands: band 3 at 9250 $cm^{-1}$ corresponds to the $d_{xy}$ → HOMO transition, while band 1 at 5200 $cm^{-1}$ is the $d_{z^2}$ → HOMO transition.

**3.1.4. Comparison with Plastocyanin.** It is important to compare the absorption and MCD spectral features of the model complex **1** with those of the blue Cu center in a prototypical blue Cu protein like plastocyanin, which are included in Figure 2.[31,32] As indicated in Figure 2, the d → d transitions are to lower energy while the LMCT bands, including the intense ($\epsilon$

(31) Gewirth, A. A.; Solomon, E. I. *J. Am. Chem. Soc.* **1988**, *110*, 3811−3819.

(32) LaCroix, L. B.; Shadle, S. E.; Wang, Y. N.; Averill, B. A.; Hedman, B.; Hodgson, K. O.; Solomon, E. I. *J. Am. Chem. Soc.* **1996**, *118*, 7755−7768.

(33) In MCD nomenclature, a $C_0$-term is Gaussian in shape and has an MCD intensity which increases as temperature decreases. This temperature dependence is due to Boltzman population of the different components of a paramagnetic ground-state split in a magnetic field. An $A_1$-term is derivative in shape and relates to the splitting of a degenerate or near-degenerate excited state in a magnetic field. It is normally temperature-independent, however, in a paramagnetic system if two excited states are near each other and spin−orbit interact this will produce *C*-terms of opposite sign and thus the same derivative shape as an $A_1$-term, but with temperature dependence (pseudo-*A*-term). The absorption intensity is given by $D_0$, and since the MCD intensity increases with an increase in absorption intensity the magnitude of the spin−orbit interaction is proportional to $C_0/D_0$, i.e., the ratio of the MCD to absorption intensity for a specific band. [Solomon, E. I.; Hanson, M. A. In *Inorganic Electronic Structure and Spectroscopy*; Solomon, E. I., Lever, A. P. B., Eds.; Wiley: New York, 1999; Vol. II, pp 1−129.

(34) Neese, F.; Solomon, E. I. *Inorg. Chem.* **1999**, *38*, 1847−1865.

(35) LaCroix, L. B.; Randall, D. W.; Nersissian, A. M.; Hoitink, C. W. G.; Canters, G. W.; Valentine, J. S.; Solomon, E. I. *J. Am. Chem. Soc.* **1998**, *120*, 9621−9631.

(36) Palmer, A. E.; Randall, D. W.; Xu, F.; Solomon, E. I. *J. Am. Chem. Soc.* **1999**, *121*, 7138−7149.

$= 5160\ M^{-1}\ cm^{-1}$[32]) S p$\pi \rightarrow$ Cu CT band at 600 nm, are to higher energy. Relative to plastocyanin, the absorption and MCD spectra of **1** are characterized by three major differences: a significant decrease in the energy of the d $\rightarrow$ d transitions (bands 1, 3−5) and a sizable increase in the intensity of the S p$\pi \rightarrow$ Cu CT transition (band 6 in Figure 2, $\epsilon$(plc) $= 5160\ M^{-1}\ cm^{-1}$[32] vs $\epsilon$(**1**) $= 6600\ M^{-1}\ cm^{-1}$ [10,12]). To higher energy there is also a noticeable decrease in the absorption intensity of the nitrogen-ligand based CT bands in the ~450 nm region: in plastocyanin the N(His) $\pi_1 \rightarrow$ Cu CT transition is more intense ($\epsilon \approx 300\ M^{-1}\ cm^{-1}$) than the pyrazole-based transitions (vide infra) in **1** ($\epsilon \approx 60\ M^{-1}\ cm^{-1}$). There is also a small red shift of the S p$\pi \rightarrow$ Cu CT band to 625 nm.[37] This shift is, however, within the range observed (590−630) in blue Cu proteins[38] and is not considered further.

The decrease in the LF band energies indicates that the site is more tetrahedral than the prototypical blue Cu site in plastocyanin. This is consistent with the crystallographic results[10,12,13] which suggest a much shorter axial N(pz) interaction (2.20 Å) than the S(Met) interaction (2.82 Å) in plastocyanin. The d $\rightarrow$ d band shifts and the tetrahedral geometric perturbation that they imply for complex **1** parallel those observed in the perturbed blue Cu protein stellacyanin.[35] We also note that the relative MCD intensities of the $d_{yz+xz}$ and $d_{yz-xz}$ transitions (bands 4 and 5) are larger than in similar Cu(II)-thiolate systems.[31,32,35,36] In **1**, the $d_{yz+xz}$ and $d_{yz-xz}$ states are much closer in energy (~250 $cm^{-1}$) than in blue Cu proteins (1200 $cm^{-1}$ − 1600 $cm^{-1}$).[31,32,35,36] Since excited-state spin−orbit coupling between these states that contributes to their MCD intensity scales inversely with the energy splitting,[34] the smaller energy splitting of these two d $\rightarrow$ d bands in **1** enhances their intensity relative to blue Cu centers.[31,32,35,36] As noted above, much of the MCD intensity of these bands cancels; overlap of bands 3 and 4 also distorts the line shape. Band 2 does not have a counterpart in plastocyanin and appears to be associated with the tris(pyrazole)hydroborate ligand (vide infra).

The increased intensity of the S p$\pi \rightarrow$ Cu CT transition in **1** relative to plastocyanin can be quantitatively expressed as the oscillator strength, *f*, which provides a measure of the transition moment ($f \propto |\langle\psi_i|\mu|\psi_f\rangle|^2$) and is proportional to the overlap of the donor and acceptor orbitals involved in the charge-transfer transition.[39] Here $\mu$ is the dipole moment operator ($\alpha\vec{r}$). From the absorption spectrum, the oscillator strength can be estimated from the expression: $f_{exp} = 4.61 \times 10^{-9}\ \epsilon_{max}\ \nu_{1/2}$, where $\epsilon_{max}$ is the maximum absorption and $\nu_{1/2}$ is the full-width at half-maximum of the peak. Using this procedure, the oscillator strength of **1** is 40% larger than for plastocyanin (0.077 for **1** vs 0.055 for plastocyanin,[36] from room-temperature absorption spectra, not shown).

**3.2. Resonance Raman Spectroscopy.** Resonance Raman (rR) spectra for **1** and analogues with related thiolates have been previously reported by Spiro, et al.[13] The vibrational spectrum of **1** in solution is characterized by a single strong peak at 421 $cm^{-1}$ that is associated with Cu−S stretching.[13,40,41] There are additional weak vibrations at 232, 322, and 500 $cm^{-1}$. Figure 3 demonstrates that the intense, 421 $cm^{-1}$ vibration in **1** is strongly resonance enhanced through the 625 nm absorption band. Importantly, the observed Cu−S stretching enhancement pattern is consistent with assignment of the 625 nm band in **1** as the S p$\pi \rightarrow$ Cu CT transition. The simplicity of the Cu−S vibrational spectrum in **1** facilitates its analysis and determination of the excited-state distortion associated with this electronic transition (vide infra).

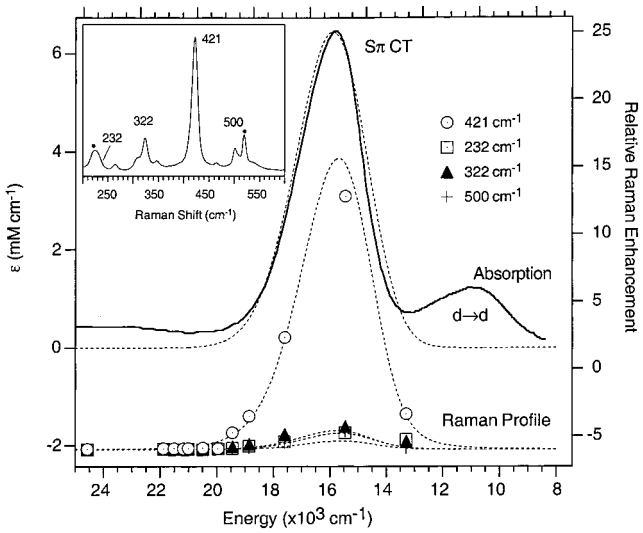


**Figure 3.** Time-domain fits[14,15,19] of the absorption spectrum[10] and resonance Raman enhancement profiles (RREP) using the parameters summarized in Table 2 for the S p$\pi \rightarrow$ Cu CT band of **1**. Inset shows a solid-state rR spectrum of **1**.[40]

**3.2.1. Comparison with Plastocyanin.** The spectrum of **1** is relatively simple compared to the complex vibrational envelope typically exhibited by blue Cu proteins such as plastocyanin in the 350−500 $cm^{-1}$ region.[42−48] The complexity of the rR spectra of blue Cu proteins has been attributed to kinematic coupling of the Cu−S stretching with various side chain modes.[49−51] With their complex vibrational envelopes, it has proven useful[42] to estimate an effective Cu−S stretching frequency for blue Cu proteins. Among the metrics used are the frequency of the most intense band[46,50] and an intensity-weighted average frequency,[42] $\langle\nu$(Cu−S)$\rangle$, where $\langle\nu$(Cu−S)$\rangle = \sum_i(I_i\ \nu_i^2)/\sum_i(I_i\ \nu_i)$.[52] The isolated Cu−S vibrational frequency

(37) There are differences in the energies and intensities of the electronic transitions over the different blue copper proteins, which have been attributed to variations in their ligation and ligand fields. See ref 35 for a detailed analysis.

(38) Solomon, E. I.; Baldwin, M. J.; Lowery, M. D. *Chem. Rev.* **1992**, *92*, 521−542.

(39) Solomon, E. I. *Commments Inorg. Chem.* **1984**, *3*, 225−320.

(40) The strong stretching feature in the rR spectra of **1** is at 421 $cm^{-1}$ in toluene and drops to 415 $cm^{-1}$ for solid-state samples. The remainder of the Raman spectrum shows no solvent effect.

(41) Randall, D. W.; George, S. D.; Holland, P. L.; Hedman, B.; Hodgson, K. O.; Tolman, W. B.; Solomon, E. I. *J. Am. Chem. Soc.* **2000**, *122*, 11632−11648.

(42) Blair, D. F.; Campbell, G. W.; Schoonover, J. R.; Chan, S. I.; Gray, H. B.; Malmström, B. G.; Pecht, I.; Swanson, B. I.; Woodruff, W. H.; Cho, W. K.; English, A. M.; Fry, H. A.; Lum, V.; Norton, K. A. *J. Am. Chem. Soc.* **1985**, *107*, 5755−5766.

(43) Woodruff, W. H.; Norton, K. A.; Swanson, B. I.; Fry, H. F. *Proc. Natl. Acad. Sci. U.S.A.* **1984**, *81*, 1263−1267.

(44) Nestor, L.; Larrabee, J. A.; Wollery, G.; Reinhammar, B.; Spiro, T. G. *Biochemistry* **1984**, *23*, 1084−1093.

(45) Han, J.; Adman, E. T.; Beppu, T.; Codd, R.; Freeman, H. C.; Huq, L.; Loehr, T. M.; Sanders-Loehr, J. *Biochemistry* **1991**, *30*, 10904−10913.

(46) Andrew, C. R.; Yeom, H.; Valentine, J. S.; Karlsson, B. G.; Bonander, N.; van Pouderoyen, G.; Canters, G. W.; Loehr, T. M.; Sanders-Loehr, J. *J. Am. Chem. Soc.* **1994**, *116*, 11489−11498.

(47) Qiu, D.; Dong, S. L.; Ybe, J. A.; Hecht, M. H.; Spiro, T. G. *J. Am. Chem. Soc.* **1995**, *117*, 6443−6446.

(48) Dong, S. L.; Spiro, T. G. *J. Am. Chem. Soc.* **1998**, *120*, 10434−10440.

(49) Czernuszewicz, R. S.; Dave, B. C.; Germanas, G. P. In *Spectroscopic Methods in Bioinorganic Chemistry*; Solomon, E. I., Hodgson, K. O., Eds.; American Chemical Society: Washington, DC, 1998; pp 220−240.

(50) Andrew, C. R.; Sanders-Loehr, J. *Acc. Chem. Res.* **1996**, *29*, 365−372.

(51) Qiu, D.; Dasgupta, S.; Kozlowski, P. M.; Goddard, W. A.; Spiro, T. G. *J. Am. Chem. Soc.* **1998**, *120*, 12791−12797.

(52) In this analysis, the 350−500 $cm^{-1}$ Raman envelope is resolved into a sum of *i* peaks, each with frequency $\nu_i$ and intensity $I_i$.

**Table 2.** Parameters for Fits of the S p$\pi \rightarrow$ Cu CT Band in **1** ($\Gamma = 500$ cm$^{-1}$)

| $\nu(i)$/cm$^{-1}$ | $\Delta(i)$ | $E_R(i)$/cm$^{-1}$ | % contrib |
|---|---|---|---|
| 421 | 3.3 | 2260 | 85 |
| 322 | 1.0 | 161 | 6 |
| 232 | 1.0 | 116 | 4 |
| 500 | 0.7 | 123 | 5 |
| | total $E_R$ | ∼2660 | |

in **1** is higher than the intensity-weighted average frequency, $\langle\nu$(Cu−S)$\rangle$ of the ∼400 cm$^{-1}$ envelope in plastocyanin (421 cm$^{-1}$ vs ∼409 cm$^{-1}$). This implies that the total Cu−S(thiolate) bonding interaction is stronger in the model complex **1** than in plastocyanin.

**3.2.2. Profile Analysis.** The resonance Raman enhancement profile (RREP) of **1** permits a quantitative estimate of the magnitude of the excited-state distortion of the Cu−S bond associated with this charge-transfer transition.[14−19,53,54] Specifically the dimensioned distortion along normal mode $Q_n$ ($\Delta Q_n$, e.g., a Cu−S stretch, with units of Å) is given by

$$\Delta Q_n = \delta \cdot \Delta \tag{1}$$

where $\Delta$ is a dimensionless normal-coordinate displacement parameter and the scaling factor, $\delta$ (Å units), is $\sqrt{\nu_n/k_n}$. Here the modal frequency is $\nu_n$ (in cm$^{-1}$) and the modal force constant, $k_n$ (in cm$^{-1}$/Å$^2$), is given by $4\pi^2c^2m_n\nu_n^2$/(hc), where $m_n$ (in grams) is the molecular reduced mass (i.e., $m_n = \mu_n/N_A$, where $N_A$ is Avogadro's number). After substitution, the scaling factor, $\delta$ (Å units), has only two variables and can be rewritten (using cgs units) as:

$$\delta = \sqrt{\nu_n/k_n} = \frac{10^8\sqrt{chN_A}}{2\pi c}\cdot\frac{1}{\sqrt{\nu_n\mu_n}} = \frac{5.805}{\sqrt{\nu_n\mu_n}} \tag{2}$$

To determine the absolute magnitude of the dimensionless normal-coordinate displacement parameter, $\Delta$, we use time-dependent Raman theory (i.e., Heller theory)[14−19] to simulate the absorption spectrum and the Raman enhancement profile with a consistent set of parameters (Figure 3). As a reasonable starting point for the simulations, the *relative* $\Delta$ values can be determined from the relative intensities of different modes in the preresonance Raman spectrum:[14,15] $I_1/I_2 \approx (\Delta_1\cdot\nu_1)^2/(\Delta_2\cdot\nu_2)^2$. During the fitting procedure, the $\Delta$ values for different vibrational modes are systematically changed such that reasonable fits are obtained for both the RREP and the UV−vis absorption spectrum (Figure 3). The parameters that successfully simulate the experimental data for **1** are summarized in Table 2. For the S p$\pi \rightarrow$ Cu CT band at 625 nm, bands at 232 cm$^{-1}$, 322 cm$^{-1}$, 500 cm$^{-1}$ are enhanced in addition to the strong enhancement of the 421 cm$^{-1}$ band with absolute $\Delta$ values of 1.0, 1.0, 0.7, and 3.3, respectively.

To approximate the vibrational system so that the excited state distortion can be determined, we consider only the Cu−S fragment and that the 421 cm$^{-1}$ mode corresponds to a stretch of this fragment. The strong relative intensity of this band in the rR spectrum in Figure 3 suggests that this is a reasonable approximation. Within this approximation, the dimensioned distortion along the normal coordinate ($\Delta Q$) relates directly to the distance change (i.e., $\Delta r = \Delta Q$). Since in the excited state, an electron is promoted into the S p$\pi$ antibonding orbital at the expense of the bonding orbital (vide infra), the distortion is an elongation along this bond. Based on this analysis, the Cu−S elongation in the S p$\pi \rightarrow$ Cu charge-transfer excited state of **1** is ∼0.20 Å. This represents an ∼10% change in the Cu−S distance in the electronic CT excited state. It is not feasible to compare the excited-state distortions of complex **1** and plastocyanin due the fact that a full normal coordinate analysis of the protein is required to account for the complex vibrational envelope that is observed in the protein.[51]

The excited-state vibrational relaxation energies of the different modes ($E_R(i)$) can be determined by relating the experimental $\Delta$ values determined above to the Huang−Rhys parameter, $S$: $S_i = E_R(i)/\nu_i = \Delta_i^2/2$.[39,53,55] Contributions of the individual modes to the relaxation energies are included in Table 2. The total vibrational relaxation energy for the S p$\pi \rightarrow$ Cu CT transition in **1** is ∼2700 cm$^{-1}$. As expected, the largest contribution (85%) to this energy is associated with the Cu−S stretching mode at 421 cm$^{-1}$. Loppnow and co-workers have used RREPs to determine the vibrational relaxation energy of the blue Cu centers in plastocyanin (1500 cm$^{-1}$) and azurin (2100 cm$^{-1}$).[56,57] In their analyses, several bands in the ∼400 cm$^{-1}$ vibrational envelope have $\Delta$ values which are similar. This confirms the distributed nature of the molecular vibration in these blue Cu centers.[51,58] Relative to plastocyanin, the ∼1200 cm$^{-1}$ larger vibrational relaxation energy of **1** indicates a stronger thiolate bonding−antibonding interaction as also indicated by the higher $\nu$(Cu−S) frequency. Finally, based on the stronger thiolate interaction in **1** than in plastocyanin revealed from XAS (vide infra), the 0.2 Å magnitude of the excited-state Cu−S distortion in **1** likely represents an upper limit for the excited-state distortion in the blue Cu centers.

**3.3. X-ray Absorption Spectroscopy.** The information available from X-ray Absorption Spectroscopy (XAS) experiments performed at the sulfur K-edge (1s $\rightarrow$ continuum), the copper L-edge (2p $\rightarrow$ continuum), and the copper K-edge (1s $\rightarrow$ continuum) provide complementary quantitative electronic structural insight.[59] Preedge features, which are due to photoexcitation of core orbitals into the HOMO, are generally of interest. The intensity of these preedge features gives electronic structural information about the HOMO,[59,60] which in model complex **1** contains some amount of S p character:

$$\Psi_{HOMO} \approx [1 - \alpha^2]^{1/2}\,|\text{Cu 3d}\rangle - \alpha\,|\text{S 3p}\rangle \tag{3}$$

The intensity of the S−K preedge feature (i.e., S 1s $\rightarrow$ HOMO, where the S 1s $\rightarrow$ S 3p transition is electric dipole allowed), provides an experimental measure of $\alpha^2$, the ligand covalency.[60] In an analogous and complementary manner, the dipole allowed Cu 2p $\rightarrow$ 3d transition observed at the Cu L-edge quantitates the Cu 3d character in the HOMO.[61] The preedge feature at the Cu K-edge derives from the dipole forbidden 1s $\rightarrow$ 3d transition, so this mostly reflects Cu 4p character mixed into the HOMO

(53) Gamelin, D. R.; Bominaar, E. L.; Mathonière, C.; Kirk, M. L.; Wieghardt, K.; Girerd, J.-J.; Solomon, E. I. *Inorg. Chem.* **1996**, *35*, 4323−4335.
(54) Henson, M. J.; Mukherjee, P.; Root, D. E.; Stack, T. D. P.; Solomon, E. I. *J. Am. Chem. Soc.* **1999**, *121*, 10332−10345.
(55) Huang, K.; Rhys, A. *Proc. R. Soc., London A* **1951**, *208*, 352.
(56) Webb, M. A.; Kwong, C. M.; Loppnow, G. R. *J. Phys. Chem. B* **1997**, *101*, 5062−5069.
(57) Fraga, E.; Webb, M. A.; Loppnow, G. R. *J. Phys. Chem.* **1996**, *100*, 3278−3287.
(58) Webb, M. A.; Loppnow, G. R. *J. Phys. Chem. A* **1999**, *103*, 6283−6287.
(59) Glaser, T.; Hedman, B.; Hodgson, K. O.; Solomon, E. I. *Acc. Chem. Res.* **2000**, in press.
(60) Hedman, B.; Hodgson, K. O.; Solomon, E. I. *J. Am. Chem. Soc.* **1990**, *112*, 1643−1645.
(61) George, S. J.; Lowery, M. D.; Solomon, E. I.; Cramer, S. P. *J. Am. Chem. Soc.* **1993**, *115*, 2968−2969.

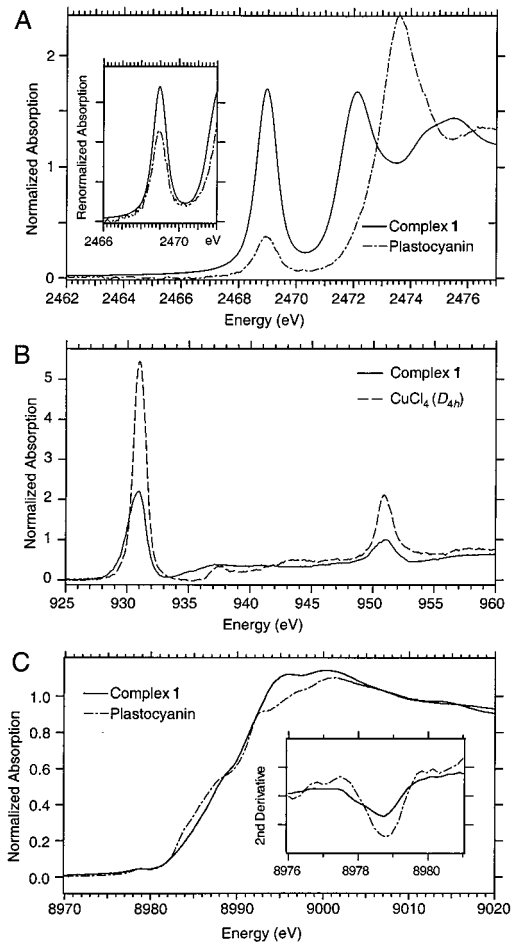


**Figure 4.** XAS spectra of complex **1** (solid trace in all panels) and relevant standards. (A) S K-edge spectra with plastocyanin.[64] (B) Cu L-edge spectra with $D_{4h}$ $[CuCl_4]^{2-}$. (C) Cu K-edge spectra with plastocyanin. Table 3 summarizes key spectral metrics.

resulting from the noncentrosymmetric character of the metal, rather than the covalency of the site. The energies of these preedge XAS features depend on the energies of the core orbitals and the HOMO.[62] The energy of the HOMO depends on two factors: the ligand field-induced splitting of the d-manifold and the effective nuclear charge, $Z_{eff}$, of the Cu. Increasing the $Z_{eff}$ of Cu places the entire d-manifold to deeper binding energy. The $Z_{eff}$ value also affects the Cu core orbital energies. Thus, in concert with MCD and absorption data, which quantitate the ligand field, the energies of the preedge features permit an evaluation of the relative $Z_{eff}$ values, while their intensities quantitate the nature of the ground-state wave function.

**3.3.1. Intensities and Comparison to Plastocyanin.** Figure 4 presents S K-edge, Cu L-edge, and Cu K-edge XAS spectra for complex **1** and relevant standards; Table 3 summarizes the Cu L-edge and S K-edge data. The renormalized S K-edge spectra, shown in the inset of Figure 4A, take into account the fact that a different number of sulfur atoms contribute to the preedge and edge features in plastocyanin.[63] This renormalized spectrum (inset Figure 4A) makes it clear that the intensity of the preedge feature in **1** is substantially greater than in plastocyanin. Quantitatively, its area is 137% larger than plastocyanin, which indicates that there is significantly more

**Table 3.** Cu L-edge and S K-edge XAS Results

| | wave function character | | preedge energies (eV) | | |
|---|---|---|---|---|---|
| | Cu L-edge | S K-edge | copper | | sulfur |
| Cu−thiolate | % Cu[a] | % S | Cu-$L_3$ | Cu-$L_2$ | S−K |
| complex **1** | 36% Cu | 52% S | 930.8 | 950.8 | 2469.0 |
| plastocyanin | 41% Cu[b] | 38% S[c] | 930.7 | ∼950.7[d] | 2469.0 |
| $D_{4h}$ $[CuCl_4]^{2-}$ | 61% Cu | | 931.0 | 951.0 | |

[a] Using Cu L-preedge areas weighted as follows: $A_{total}$ = Area($L_3$) + Area($L_2$). [b] Reference 61. [c] Reference 64. [d] $L_2$ preedge energy not given in ref 61.

thiolate S p character in the HOMO of **1** than in plastocyanin. Previous studies indicate 38% S p character in the HOMO of plastocyanin,[64] which gives the amount of S p character in the HOMO of model complex **1** as 52%. Thus, these XAS results point to a more covalent Cu−thiolate interaction in **1** than in plastocyanin.

The L-edge XAS experiment quantitates the complementary Cu d character in the HOMO.[61] The intensity of the preedge area in **1** is smaller than that of $D_{4h}$ $[CuCl_4]^{2-}$, which corresponds to 61% Cu character (Figure 4B). This indicates that there is less Cu d character in the HOMO of **1** than in $D_{4h}$ $[CuCl_4]^{2-}$. Quantitatively, the HOMO of **1** contains 36% Cu d character, which is somewhat less than in plastocyanin (41% Cu)[61] and consistent with the increased S p character observed with S K-edge XAS. Thus, relative to plastocyanin there is a redistribution of electron density from the Cu to the S(thiolate) ligand in **1**. Presumably the remaining wave function character in **1** (∼11%) resides on the tris(pyrazolyl)hydroborate and triphenylmethyl ligands. This residual wave function character is somewhat less than in plastocyanin (∼21%), suggesting the N covalency in **1** is somewhat smaller than that observed in blue Cu centers such as plastocyanin.

**3.3.2. Energies and Comparison to Plastocyanin. Sulfur Edge and Preedge Energies.** As revealed in Figure 4A, the feature in the S K-edge at ∼2472 eV appears to shift dramatically (>1 eV) between plastocyanin and complex **1**. However, this shift does not represent an actual shift of the edge (1s → 4p transition), rather it reflects a transition to another bound state, possibly the S−C antibonding orbital in the triphenylmethylthiolate ligand.[65] Thus, since plastocyanin and **1** involve different thiolate ligands, it is not possible to determine an accurate edge position. As indicated in Figure 4 and summarized in Table 3, the XAS preedge features for **1** and plastocyanin are at the same energy (2469.0 eV). From the MCD and absorption results described above, the ligand field in **1** is reduced relative to plastocyanin, which would decrease the S K-preedge transition energy. However, the S 1s core energy in **1** is expected to be stabilized to deeper binding energy due to its increased covalency,[62] which would increase the preedge transition energy. The combination of these offsetting effects results in similar energies for the 1s → HOMO preedge transitions for these two copper−thiolate centers.

**Cu Preedge Energies: L-edge.** The Cu 2p → 3d transition is split into $L_3$ and $L_2$ components due to spin−orbit coupling. Figure 4B shows preedge features of the Cu L-edge spectrum of **1** at 930.8 eV ($L_3$) and 950.8 eV ($L_2$) in comparison with $D_{4h}$ $[CuCl_4]^{2-}$. These preedge energies are approximately 0.1 eV higher in energy than for plastocyanin (Table 3).[61] The observed small shift to higher energy, along with the weaker

(62) Shadle, S. E.; Hedman, B.; Hodgson, K. O.; Solomon, E. I. *Inorg. Chem.* **1994**, *33*, 4235−4244.

(63) There are three sulfurs in plastocyanin (Met57, Cys84, and Met92) which all contribute to the edge jump, while only the Cys thiolate contributes preedge intensity.[64]

(64) Shadle, S. E.; Penner-Hahn, J. E.; Schugar, H. J.; Hedman, B.; Hodgson, K. O.; Solomon, E. I. *J. Am. Chem. Soc.* **1993**, *115*, 767−776.

(65) Glaser, T.; Rose, K.; Shadle, S. E.; Hedman, B.; Hodgson, K. O.; Solomon, E. I. *J. Am. Chem. Soc.* **2000**, *submitted*.

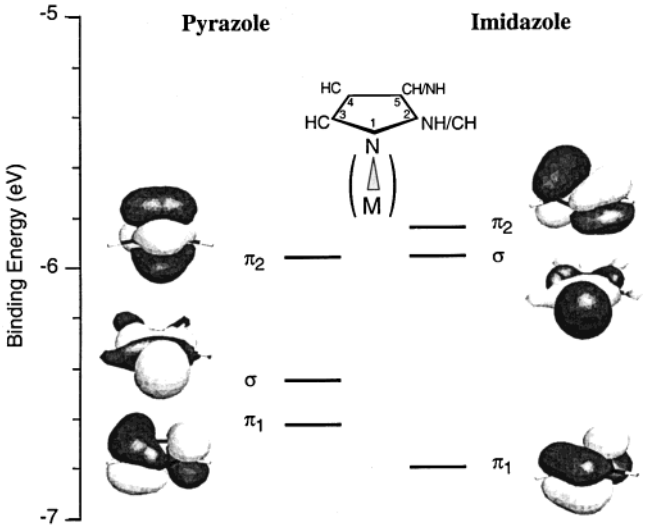


**Figure 5.** Comparison of the calculated energy level diagram and orbital representations for the valence orbitals of pyrazole (left) and imidazole (right). Wave function descriptions are presented in Table 4.

ligand field in **1**, which would produce a preedge energy shift to lower energy (all other factors being equal), suggests a higher effective nuclear charge ($Z_{eff}$) on Cu in the model complex relative to plastocyanin that shifts the core Cu 2p orbital to deeper binding energy.

**Cu K-edge.** Figure 4C compares the Cu K-edge XAS spectra for plastocyanin and complex **1**. The inset of Figure 4C, which shows the second derivatives in the preedge region, indicates that the Cu K-preedge features (Cu 1s → 3d transition) in plastocyanin and complex **1** are at similar energies (8978.8 eV). In stellacyanin, which like **1** is tetragonally distorted relative to plastocyanin and therefore also has a smaller ligand field splitting,[35] an 0.5 eV decrease in the Cu K-preedge transition was observed.[66] For stellacyanin relative to plastocyanin, the effects of a decreased $Z_{eff}$ and a decreased ligand field reinforced each other and lead to an 0.5 eV decrease in the transition energy.[66] The similarity of the Cu K-preedge transition energies for plastocyanin and **1** therefore suggests that for model complex **1** the effects on the transition energy of the changes in $Z_{eff}$ and ligand field may cancel. This implies a lower $Z_{eff}$ for plastocyanin than for the model complex, consistent with the Cu L-edge results.

**3.4. Calculations.**

**3.4.1. Electronic Structures of Pyrazole versus Imidazole.** For a comparison of the electronic structure of **1** to plastocyanin, we first consider the electronic structure of the pyrazole and imidazole nitrogen donors. Figure 5 compares the energies and contours for the high-energy valence orbitals of these ligands that can interact with the Cu. The wave functions are summarized in Table 4. As Figure 5 demonstrates, the orbital pattern is somewhat similar for both free ligands in that there are two out-of-plane $\pi$-type orbitals ($\pi_1$ and $\pi_2$) and one in-plane $\sigma$-type orbital (N$\sigma$), which lies between the two $\pi$-type orbitals. The energies of the orbitals are similar with the $\pi_1 - \pi_2$ splitting slightly reduced for pyrazole relative to imidazole ($E(\pi_1) - E(\pi_2) = 0.67$ eV for pyrazole vs 0.96 eV for imidazole, Figure 5). The N$\sigma$ donor orbitals for these two ligands are important for bonding to the metals by which they are greatly stabilized in energy, though by similar amounts. The N$\sigma$ levels in the free ligands exhibit similar character for the coordinating nitrogens, 76% in pyrazole versus 79% in imidazole, which suggests that imidazole and pyrazole are similar donor ligands, though pyrazole could be slightly weaker. The pyrazole N$\sigma$ orbital is ~0.5 eV lower in energy than in imidazole, which could also make it a slightly poorer donor to Cu due to a greater energy denominator. There is, however, an important difference between wave functions of the $\pi_1$ and $\pi_2$ levels in imidazole and pyrazole. In imidazole, the highest-energy $\pi_2$ orbital has little N character (8%) on the N atom available for metal ligation. In contrast, for pyrazole the $\pi_2$ orbital has substantial N character (34%) on the N atom available for metal ligation. The situation is reversed for the $\pi_1$ orbitals to deeper binding energy: in imidazole the potentially ligating N has significant wave function character (40%), while the analogous atom in pyrazole has much less (7%) ligating N character. When three pyrazoles are combined to make tris(pyrazolyl)hydroborate, three sets of the three types of orbitals ($\sigma$, $\pi_1$, $\pi_2$) are obtained to give a total of nine pyrazole-based orbitals. In **1**, the ligand exhibits $C_1$ symmetry and there is some mixing between the $\pi_1$ and $\pi_2$ orbitals. Upon complexation to the Cu in **1**, the $\sigma$-derived orbitals are stabilized to substantially deeper energy due to bonding, which leaves the six $\pi_1$ and $\pi_2$ levels as the low-energy valence orbitals for this ligand.

**Table 4.** Calculated Orbital Characters for Free Pyrazole and Imidazole

| pyrazole | | | | imidazole | | | |
|---|---|---|---|---|---|---|---|
| | orbital: | | | | orbital: | | |
| *E* (eV) | −6.63 | −6.45 | −5.96 | *E* (eV) | −6.80 | −5.96 | −5.84 |
| atom[a] | $\pi_1$ | $\sigma$ | $\pi_2$ | atom[a] | $\pi_1$ | $\sigma$ | $\pi_2$ |
| N1 | 7.2 | 75.6 | 34.1 | N1 | 40.2 | 78.8 | 8.4 |
| N2 | 31.4 | 3.8 | 2.2 | C2 | 0.6 | 5.1 | 28.3 |
| C3 | 38.0 | 7.2 | 0.7 | C3 | 22.7 | 4.8 | 19.4 |
| C4 | 17.2 | 4.7 | 28.1 | C4 | 0.8 | 4.4 | 39.8 |
| C5 | 3.4 | 3.7 | 32.0 | N5 | 32.9 | 2.0 | 1.2 |
| H | 2.3 | 3.3 | 1.8 | H | 1.6 | 4.0 | 2.5 |

[a] Atom numbering scheme illustrated in Figure 5.

**3.4.2. Electronic Structure of the Thiolate.** For free methylthiolate or triphenylmethylthiolate, there are two almost degenerate ($\Delta E < 0.1$ eV) sulfur-based valence orbitals at low binding energy available for interaction with the metal. In the free ligand, these two orbitals are derived from the two p orbitals perpendicular to the S−C bond. To substantially (2−3 eV) deeper binding energy lies the orbital involved in the S−C $\sigma$ interaction, which is not expected to be significantly involved in the Cu−S(thiolate) bond, and therefore not considered further. When the S(thiolate) interacts with a metal center, the Cu−S−C angle splits these two levels into an S p$\pi$ orbital, with orbital lobes that are perpendicular to the Cu−S−C plane, and an S p pseudo-$\sigma$ orbital, with orbital lobes that are located in this plane, but perpendicular to the S−C bond. The S p$\pi$ orbital will have a $\pi$-type interaction with the Cu d-orbitals, while the other will have a pseudo $\sigma$-type interaction where one of the S p orbital lobes interacts with a Cu d orbital lobe. States involving both of these types of S p orbitals are observed in the spectroscopy of **1** (vide supra).

**3.4.3. Electronic Structure of Complex 1.** For complex **1**, Figure 6 presents an energy level diagram along with representations of the highest valence orbitals derived from the nonlocal gradient-corrected (i.e., generalized gradient approximation, GGA) DFT implemented in the ADF package.[25,26] Figure 7 shows contours for the key orbitals involved in the thiolate−Cu bonding interaction. The wave function characters of **1** derived from this calculation are summarized in Table 5.

(66) DeBeer, S.; Randall, D. W.; Nersissian, A. M.; Valentine, J. S.; Solomon, E. I. *J. Phys. Chem.* **2000**. In Press.

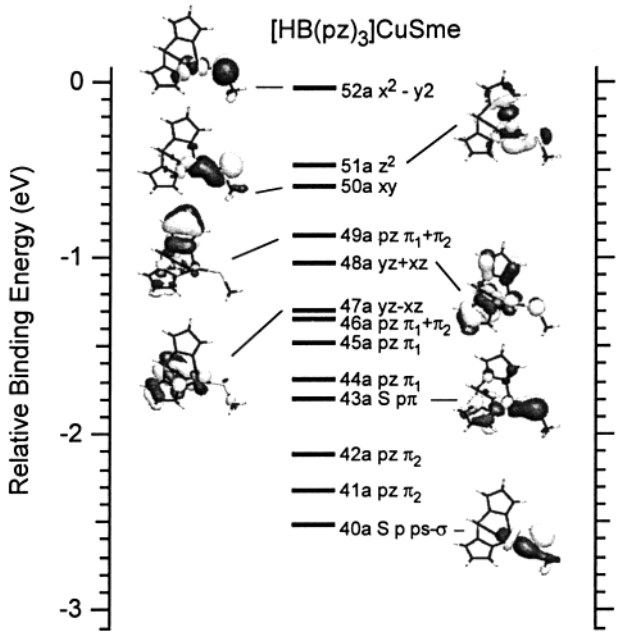


**Figure 6.** Calculated energy level diagram and selected orbital representations for the occupied, high-lying valence orbitals of complex **1**. See Table 5 for a summary of the calculated wave function characters.

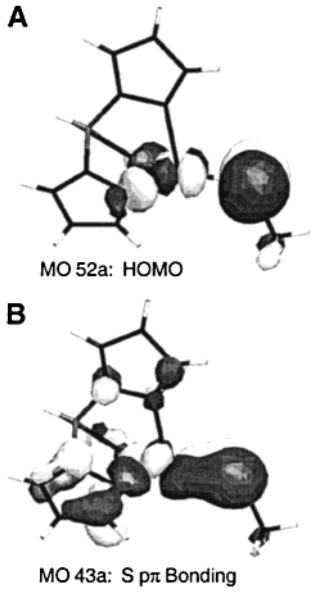


**Figure 7.** Contours for the thiolate−Cu bonding and antibonding orbitals of **1**: (A) Cu $d_{x^2-y^2}$ HOMO (52A) showing the S p$\pi$ antibonding and N $\sigma$ antibonding interactions; (B) S p$\pi$ bonding orbital (43A).

**3.4.3.1. HOMO.** The redox-active, half-occupied HOMO calculated for **1** shows a $\pi$-type interaction between the Cu $d_{x^2-y^2}$ orbital and the thiolate S p$\pi$ orbital (Figure 7A). This HOMO pattern is observed in blue Cu centers such as plastocyanin.[31,32,67−69] In analogy to blue Cu proteins, this interaction is calculated to be very covalent with 34% Cu and 49% S character in this orbital (Table 5). The Cu $d_{x^2-y^2}$ character calculated for the HOMO is consistent with the *g*-value pattern of $g_{\|} > g_{\perp} > g_e$ (=2.0023). Further, there is very little Cu $d_{z^2}$ character mixed into the HOMO consistent with the axial EPR spectrum that is observed.[10,11,70] These calculations also reasonably reproduce the Cu character observed with the Cu L-edge XAS experiments (34% $Cu_{calc}$ vs 36% Cu from Cu L-edge XAS). The thiolate S p character is also in reasonable agreement with that observed from the S K-edge experiments (49% $S_{calc}$ vs 52% S from S K-edge XAS). Calculations for both methylthiolate and triphenylmethylthiolate complexes give similar total S characters. In addition to the dominant thiolate $\pi$-type interaction, there is also a $\sigma$-type interaction between the equatorial pyrazole ligands and the Cu $d_{x^2-y^2}$ lobes. Finally, the axial pyrazole ligand has very little contribution to the HOMO.

**3.4.3.2. Excited Electronic States. Spectral Patterns and Assignments for 1.** The calculated one-electron orbital energy ordering in Table 5 reflects experimental observations and spectroscopic assignments. To deeper binding energy than the HOMO lie the Cu $d_{z^2}$ and Cu $d_{xy}$ orbitals, the latter having an antibonding interaction with the thiolate pseudo-$\sigma$ orbital. Orbital 49A, which lies below these, is characterized as a ligand-based orbital whose density is localized on the pyrazole ligand. These calculations suggest that band 2 in Figure 2B likely results from a transition from this high-energy pyrazole-based orbital (49A) to the HOMO.[71] This orbital is best characterized as a mixture of $\pi_1$ and $\pi_2$ on the axial pyrazole ligand. Completing the ligand field manifold are the Cu $d_{yz+xz}$, $d_{yz-xz}$ orbitals at deeper energy that exhibit a small antibonding interaction between the metal and the $\pi_1$ orbitals on the equatorial pyrazole ligands. Below the d → d block lie three additional pyrazole based orbitals. The first of these (46A) shows a mixture of $\pi_1$ and $\pi_2$ character on all three ligating pyrazoles, while the next two levels (44A and 45A) are mostly $\pi_1$ in nature and localized on the equatorial pyrazole ligands. Transitions from these pyrazole-based orbitals to the Cu $d_{x^2-y^2}$ HOMO, though expected to be relatively weak in the MCD, may further complicate the spectral pattern observed in the band 4, 5 (Cu $d_{yz\pm xz}$) region (vide supra). At deeper energy is the S p$\pi$ - Cu $d_{x^2-y^2}$ bonding orbital (Figure 7B), which is involved in the intense S p$\pi$ → Cu CT transition observed at 625 nm. The intensity of this band is due to the significant ligand-ligand overlap between the S p$\pi$ - Cu $d_{x^2-y^2}$ bonding orbital and the HOMO, where the interaction is antibonding. Next lie the remaining two pyrazole $\pi_1$ orbitals, which are localized on the equatorial ligands and have some bonding interactions with the $d_{xz\pm yz}$ pair. Note that the pyrazole $\pi_1$ and $\pi_2$ orbital energy pattern observed in the calculation is altered from that observed in the free ligand (Figure 5), due to the bonding interaction of the $d_{xz,yz}$ pair and the $\pi_1$ orbitals. These pyrazole ligands have less than 8% wave function character on any one of the ligating nitrogens (Table 5). Finally, the S p pseudo-$\sigma$ orbital, which is calculated to lie below these pyrazole-based orbitals, shows a bonding interaction with the Cu $d_{xy}$ orbital. For complex **1** the calculations, thus, predict a spectral pattern with the ligand field block to lowest energy, but interspersed with various pyrazole-based orbitals, followed by the CT transitions involving the S p$\pi$, S pseudo-$\sigma$, and pyrazole-based orbitals. The implications of the high thiolate covalency on the intensity of the S pseudo-$\sigma$ → Cu CT transition are considered in the discussion.

**Comparison with Plastocyanin.** For comparison with these computational results on complex **1**, a parallel nonlocal gradient DFT calculation was performed for plastocyanin using the ADF package. This calculation is summarized in Table S1 (see

(67) Penfield, K. W.; Gewirth, A. A.; Solomon, E. I. *J. Am. Chem. Soc.* **1985**, *107*, 4519−4529.
(68) Larsson, S.; Broo, A.; Sjölin, L. *J. Phys. Chem.* **1995**, *99*, 4860−4865.
(69) Pierloot, K.; Dekerpel, J. O. A.; Ryde, U.; Roos, B. O. *J. Am. Chem. Soc.* **1997**, *119*, 218−226.
(70) Gewirth, A. A.; Cohen, S. L.; Schugar, H. J.; Solomon, E. I. *Inorg. Chem.* **1987**, *26*, 1133−1146.
(71) Studies on the related complex, $[HB(pz')_3]CuSC_6F_5$, show a generally similar MCD pattern in the low-energy region consistent with this assignment. See Figure S1, Supporting Information.

**Table 5.** Results of ADF Calculations for the $C_1$ $[HB(pz)_3CuSCH_3]^0$ Approximation to **1**

| | energy (eV) | −4.72 | −5.16 | −5.29 | −5.56 | −5.72 | −5.98 | −6.04 | −6.17 | −6.38 | −6.49 | −6.80 | −7.01 | −7.21 |
|---|---|---|---|---|---|---|---|---|---|---|---|---|---|---|
| | orbital labels | **52A** | **51A** | **50A** | **49A** | **48A** | **47A** | **46A** | **45A** | **44A** | **43A** | **42A** | **41A** | **40A** |
| | | HOMO | $z^2$ | $xy$ | pz $\pi_1+\pi_2$ | $yz+xz$ | $yz-xz$ | pz $\pi_1+\pi_2$ | pz $\pi_1$ | pz $\pi_1$ | S$\pi$ CT | pz $\pi_2$ | pz $\pi_2$ | S p ps. $\sigma$ |
| **Cu** | Cu S+P total | 0.2 | 7.1 | 7.8 | 0.0 | 0.3 | 0.8 | 0.0 | 1.5 | 0.1 | 3.5 | 0.3 | 0.5 | 0.6 |
| | $d_{z^2}$ | 0.1 | 37.4 | 7.2 | 0.1 | 0.2 | 6.8 | 0.0 | 0.1 | 1.5 | 0.3 | 0.1 | 11.1 | 17.8 |
| | $d_{yz}$ | 0.1 | 0.1 | 6.4 | 1.1 | 12.5 | 11.0 | 1.8 | 1.0 | 2.3 | 5.1 | 27.0 | 11.7 | 18.6 |
| | $d_{xz}$ | 0.2 | 0.1 | 6.4 | 1.2 | 13.5 | 13.3 | 1.9 | 1.2 | 2.4 | 5.5 | 27.5 | 12.3 | 18.7 |
| | $d_{xy}$ | 0.1 | 13.2 | 12.4 | 0.1 | 0.3 | 1.8 | 0.0 | 0.1 | 1.0 | 0.2 | 0.1 | 19.2 | 6.0 |
| | $d_{x^2-y^2}$ | 32.9 | 0.0 | 0.1 | 0.1 | 1.2 | 0.1 | 0.0 | 4.9 | 0.3 | 18.0 | 0.2 | 0.3 | 0.3 |
| | **Cu d total** | **33** | **51** | **32** | **3** | **28** | **33** | **4** | **7** | **7** | **29** | **55** | **55** | **61** |
| | Cu all total | 34 | 58 | 40 | 3 | 28 | 34 | 4 | 9 | 8 | 33 | 55 | 55 | 62 |
| **S** | **S total** | **49** | **10** | **46** | **1** | **7** | **2** | **0** | **10** | **1** | **22** | **0** | **2** | **31** |
| | $CH_3$ | 2 | 1 | 2 | 0 | 0 | 2 | 0 | 0 | 0 | 0 | 0 | 1 | 2 |
| **Neq**[a] | **N lig**[a] | **6** | **2** | **3** | **1** | **4** | **11** | **8** | **2** | **1** | **4** | **6** | **6** | **0** |
| | N (B)[a] | 0 | 0 | 0 | 3 | 1 | 2 | 2 | 8 | 19 | 1 | 2 | 2 | 0 |
| | pz − N lig[a] | 1 | 2 | 2 | 8 | 7 | 27 | 16 | 19 | 50 | 3 | 12 | 11 | 0 |
| | pz total | 7 | 4 | 4 | 9 | 11 | 38 | 24 | 21 | 51 | 7 | 18 | 17 | 0 |
| **Neq** | **N lig** | **5** | **2** | **3** | **1** | **9** | **6** | **7** | **2** | **1** | **8** | **5** | **8** | **0** |
| | N (B) | 0 | 0 | 0 | 3 | 3 | 0 | 1 | 10 | 10 | 5 | 2 | 2 | 0 |
| | pz − N lig | 0 | 2 | 0 | 9 | 18 | 11 | 12 | 30 | 29 | 14 | 8 | 12 | 0 |
| | pz total | 6 | 4 | 3 | 10 | 27 | 17 | 18 | 32 | 30 | 22 | 13 | 20 | 0 |
| **Nax** | **N lig** | **0** | **16** | **2** | **12** | **6** | **1** | **12** | **0** | **0** | **2** | **4** | **1** | **0** |
| | N (B) | 0 | 0 | 0 | 13 | 3 | 0 | 11 | 5 | 1 | 3 | 2 | 0 | 0 |
| | pz (ax) − N lig | 0 | 0 | 0 | 60 | 16 | 1 | 36 | 20 | 2 | 8 | 7 | 0 | 0 |
| | pz (ax) total | 0 | 17 | 2 | 72 | 21 | 2 | 48 | 20 | 3 | 9 | 11 | 1 | 0 |
| **HB** | | **0** | **0** | **0** | **1** | **0** | **0** | **0** | **0** | **0** | **0** | **0** | **0** | **0** |

[a] N lig denotes the Cu-ligating nitrogen in the pyrazole rings; N(B) denotes the nonligating N in the pyrazole rings (bound to B); pz − N lig indicates the total wave function character for nonligating atoms for each pyrazole ring.

Supporting Information). Consistent with experiment and previous calculations,[31,32,67−69] the HOMO of plastocyanin is calculated to involve a covalent antibonding interaction between the Cu $d_{x^2-y^2}$ and S p$\pi$ orbitals, which is calculated to be more covalent than observed experimentally with S K-edge XAS (54% $S_{calc}$ vs 38% S from S K-edge XAS).[64] Generally the pattern of excited states is similar to that reported for blue Cu centers[31,32,35,36] and largely parallels the above assignment for **1**. In agreement with the experimentally observed change in ligand field transition energies from the MCD spectral data, however, the d manifold in plastocyanin is calculated to be less compressed than in **1**. As in complex **1**, the d manifold for plastocyanin is interspersed with imidazole-based orbitals. In contrast to **1**, however, in plastocyanin these imidazole-based levels have little character on the ligating nitrogen (<2%) and are, therefore, not expected to contribute to the absorption or MCD intensity. In contrast, the low-energy, pyrazole-based level (49A) in complex **1** shows more ligating nitrogen wave function character, which, as discussed above, appears to be the origin of low-energy band 2 observed in the MCD spectrum of the model complex that does not have a counterpart in plastocyanin. In this plastocyanin calculation, the d manifold is followed to deeper energy by CT transitions: the S p$\pi$ → Cu CT transition (the origin of the "blue" band at 600 nm), the S p pseudo-$\sigma$ → Cu transition, two imidazole-based $\pi_1$ → Cu CT transitions, and a Met → Cu CT transition. In plastocyanin, the nitrogen ligand based orbitals at deep binding energy, which give rise to the weak CT transitions in the ∼450 nm region, have substantially more wave function character on the ligating nitrogen than their counterparts in complex **1**: ∼35% N(imidazole) in plastocyanin versus ∼6% N(pyrazole) in **1** (Table 4 vs Table S1 in the Supporting Information).

## 4. Discussion

**4.1. Effects of Covalency.** Model complex **1** successfully reproduces many spectral features of blue Cu proteins,[10−12] such as plastocyanin,[8] including the characteristic blue band at ∼600 nm. This complex reasonably reproduces the geometry of the protein site by using appropriate synthetic analogues for the equatorial histidine ligands and the cysteine thiolate. There are important differences between the model complex and the blue Cu site in plastocyanin, however. These differences derive from two features of the site: most importantly, the comparatively stronger thiolate donor interaction in **1** but also the replacement of the imidazoles and axial S(Met) by pyrazole ligands. The XAS experiments presented in Figure 4 clearly demonstrate that the thiolate in **1** interacts more strongly than the cysteinate in plastocyanin. This leads to an extremely covalent HOMO in **1** with, remarkably, *increased* S(thiolate) character relative to plastocyanin (52% S vs 38% S). This dramatic change in covalency affords the opportunity to investigate how the increased thiolate covalency in **1** affects other spectroscopic properties of the site. This enables us to evaluate many earlier suggestions regarding the important influences of this covalent bond upon the electronic structure and spectra of the blue Cu site.

**4.1.1. Optical Spectroscopy: Absorption and RREP.** First, the presence of an intense, low-energy CT band in **1** indicates that its HOMO is characterized by a $\pi$-type interaction between the S p orbital and the Cu $d_{x^2-y^2}$ orbital, consistent with the ground-state electronic structure of plastocyanin.[8] Importantly, the oscillator strength of this band in **1** is higher than in plastocyanin. Since the intensity of CT transitions originates from overlap of ligand orbitals in the donor and acceptor levels, this is qualitatively consistent with the increased thiolate covalency in the HOMO of complex **1**. Baldwin, et al.[72] have outlined a semiquantitative procedure whereby the relative ligand covalency in the HOMO (i.e., $\alpha^2$ in eq 3) of different sites may be estimated from the oscillator strength ($f_{exp}$), the charge-transfer transition energy ($\nu_{CT}$), and the ligand−metal bond length ($r_{ML}$) according to the relationship: $\alpha^2 \propto f_{exp}/[\nu_{CT}\,(r_{ML})^2]$. This result is based on calculations[73,74]

(72) Baldwin, M. J.; Root, D. E.; Pate, J. E.; Fujisawa, K.; Kitajima, N.; Solomon, E. I. *J. Am. Chem. Soc.* **1992**, *114*, 10421−10431.
(73) Ros, P.; Schuit, G. C. A. *Theor. Chim. Acta (Berlin)* **1966**, *4*, 1−12.
(74) van der Avoird, A.; Ros, P. *Theor. Chim. Acta (Berlin)* **1966**, *4*, 13-21.

that indicate that the majority of CT intensity derives from the "ligand−ligand" term in the expansion of the transition moment, $[\langle\psi^{D}|\ r\ |\ \psi^{A}\rangle]^2$, where the D and A superscripts indicate the electron donor and acceptor states involved in the transition. From this CT band intensity analysis,[72] the thiolate covalency of the model complex is larger than that of plastocyanin by a factor of 1.38, which is within the error of the value derived from S K-edge XAS (52%/38% ≈ 1.37). The substantial thiolate covalency of the site measured with S K-edge XAS is, thus, quantitatively consistent with the very high intensity of the S(thiolate) → Cu CT transition.

Further, the weak charge-transfer bands at ∼450 nm in **1** do not show increased intensity associated with the substantial increase in thiolate covalency. Rather these bands show a 4-fold *decrease* in intensity relative to the analogous bands in plastocyanin. Contrary to suggestions in the literature,[75,76] this implies that these high-energy bands in the plastocyanin absorption spectrum are not due to the S p pseudo-$\sigma$ → HOMO CT transition, as is clearly the case for some perturbed blue Cu centers.[32,35] In plastocyanin and complex **1**, the S p pseudo-$\sigma$ → Cu CT transition appears to lie to just higher energy than (and overlaps with) the S p$\pi$ → Cu CT transition, as assigned in Figure 2 (band 7) and Table 1 as well as elsewhere in the literature.[31,32,35,36]

The time-domain analysis of the RREP data points to further differences between the electronic structure of plastocyanin and complex **1**. The vibrational relaxation energy, $E_R$, associated with the S p$\pi$ → Cu CT band is larger for the model complex than plastocyanin[57] by 1200 $cm^{-1}$. This points to a stronger thiolate−Cu bonding−antibonding interaction in **1** than in plastocyanin. Because of the increased covalency observed in the XAS experiments, the ∼0.20 Å excited-state distortion derived for **1** likely represents an upper limit for the excited-state distortion of the Cu−S bond in blue Cu centers. The Cu−S stretching frequency in the Raman spectra also suggests a stronger Cu−S bond in **1** than in plastocyanin: in **1** the Cu−S stretching frequency is 421 $cm^{-1}$,[13] while in plastocyanin the average frequency $\langle\nu_{Cu-S}\rangle$ is 409 $cm^{-1}$. Thus, both the oscillator strength derived from the absorption spectrum and the Cu−S stretching frequency and excited-state distortion from Raman are entirely consistent with and expected from the increased thiolate covalency of **1** relative to plastocyanin that is observed in the S K-edge XAS spectra.

**4.1.2. EPR Comparison of 1 to Plastocyanin.** It is also useful to compare the EPR spectrum of **1** to those of blue Cu proteins. Complex **1** is characterized by an axial EPR spectrum with $g_{\|}$ of 2.23,[11,12] which very closely matches the EPR $g_{\|}$ value observed for plastocyanin ($g_{\|} = 2.226$).[77] With the increased covalency of **1** relative to plastocyanin it might be expected that $\Delta g_{\|}$ ($= g_{\|} - g_e$) should be less for **1** than for plastocyanin. However, the $\Delta g_{\|}$ value is also proportional to the energy difference between the HOMO and the Cu $d_{xy}$ orbital ($E_{xy}$) with which the HOMO can spin−orbit couple through the $L_z$ operator (i.e., $\Delta g_{\|} \propto 1/E_{xy}$). The $E_{xy}$ value for **1** is 1600 $cm^{-1}$ lower than in plastocyanin (Figure 2). In the tetrahedrally distorted blue Cu center in the protein stellacyanin, a similar shift in the d → d transition energies was sufficient to substantially *increase* the $\Delta g_{\|}$ value compared to plastocyanin.[35] Thus, the reduced ligand field in **1** offsets the expected decrease in $\Delta g_{\|}$ due to covalency. This gives $\Delta g_{\|}$ values that are the same for plastocyanin and **1** and is consistent with the presence of more covalent Cu−S(thiolate) interaction in **1**.

The reduction in the Cu $A_{\|}$ value in plastocyanin ($A_{\|} \approx 63 \times 10^{-4}$ $cm^{-1}$) relative to normal Cu complexes ($A_{\|} \approx 140 \times 10^{-4}$ $cm^{-1}$) is often cited as evidence for the covalency of the blue Cu site. The hyperfine is similar for complex **1** ($A_{\|} \approx 66 \times 10^{-4}$ $cm^{-1}$) and plastocyanin, while the thiolate covalency of **1** is larger than plastocyanin. However, the Cu L-edge XAS data indicates that the Cu character is, in fact, similar for **1** and plastocyanin (36% vs 41%). This suggests that the three pyrazole ligands in **1** constitute a poorer donor set than the $N(His)_2S$-(Met) donor set in plastocyanin for which the increased thiolate covalency in **1** compensates. This is supported by the comparison of pyrazole versus imidazole ligation below.

**4.2. Imidazole versus Tris(Pyrazole) Copper Ligation.** The Cu L- and K-edge XAS results imply that $Z_{eff}$ for complex **1** is higher than for plastocyanin, which suggests that the $N(His)_2S$-(Met) donor set is stronger than that of tris(pyrazolyl)hydroborate. As discussed above, the total XAS intensities for the model complex also suggest that there is less N donor character in the HOMO wave function of **1** than in plastocyanin. This is consistent with and a dominant contribution to the increased thiolate donor strength in **1** relative to plastocyanin. Inspection of the crystal structures of plastocyanin and **1** indicates that in complex **1** there is a small but consistent decrease of ∼10°−15° from the ideal N−N−Cu (C−N−Cu in imidazole) angles of ∼126°, which is invariably observed in plastocyanin and other blue Cu proteins.[7,78−80] This angular deviation in **1** corresponds to a rotation about the normal of the pyrazole plane that directs its $\sigma$ donor orbital (vide supra) away from the Cu. Calculations have been performed to minimize the geometry of an analogue of **1**, where the boron is removed and the N(pz)−B bonds are replaced with N(pz)−H bonds. Upon eliminating the N(pz)−B bonds, while there are no significant bond length changes, the N−N−Cu angles revert to the ideal 126°. The source of this orbital misdirection of the pyrazole N$\sigma$ donor in tris(pyrazolyl)-hydroborate, which weakens the effective donor strength of the ligand, involves the restraining pyrazole−boron interaction that appears to somewhat constrain the N−Cu interaction.

While the constrained geometry of the tripodal tris(pyrazolyl)-hydroborate ligand is an important contributor to the higher $Z_{eff}$ for Cu in **1** relative to plastocyanin, the differences between pyrazole and imidazole ligation also give **1** distinctive changes in the spectroscopic features. Perturbations of the N-based ligand in **1** relative to plastocyanin can help to assign imidazole-based features in the spectra of the latter. As noted in Figure 2A, there is a decrease in the absorption intensity in the ∼450 nm region in **1** relative to plastocyanin. This suggests that in plastocyanin there is absorption intensity in this region that derives from imidazole ligand $\pi_1$ → HOMO CT transitions (and an S(Met) → Cu CT transition[31,32,77]) and not the S p pseudo-$\sigma$ → Cu CT transition. In plastocyanin, the intensity of these bands is not strong due to small ligand orbital overlap between the donor and acceptor MOs. In stellacyanin, this transition is stronger,[35] which could result from the tetrahedral distortion of the site with equatorial imidazole ligands, which would increase the N(His) $\pi$ overlap. The calculations support this assignment: the $\pi_1$ levels in plastocyanin are calculated to contain 35% character

(75) Han, J.; Loehr, T. M.; Lu, Y.; Valentine, J. S.; Averill, B. A.; Sanders-Loehr, J. *J. Am. Chem. Soc.* **1993**, *115*, 4256−4263.
(76) Pierloot, K.; DeKerpel, J. O. A.; Ryde, U.; Olsson, M. H. M.; Roos, B. O. *J. Am. Chem. Soc.* **1998**, *120*, 13156−13166.
(77) Penfield, K. W.; Gay, R. R.; Himmelwright, R. S.; Eickman, N. C.; Norris, V. A.; Freeman, H. C.; Solomon, E. I. *J. Am. Chem. Soc.* **1981**, *103*, 4382−4388.
(78) Baker, E. N. *J. Mol. Biol.* **1988**, *203*, 1071−1095.
(79) Nar, H.; Messerschmidt, A.; Huber, R.; Kamp, M. v. d.; Canters, G. W. *J. Mol. Biol.* **1991**, *221*, 765−772.
(80) Hart, P. J.; Nersissian, A. M.; Herrmann, R. G.; Nalbandyan, R. M.; Valentine, J. S.; Eisenberg, D. *Protein Sci.* **1996**, *5*, 2175−2183.

on the ligating nitrogens (Table S1), while the $\pi_2$ levels, which are in this region in **1** due to bonding interactions with the Cu $d_{yz+xz}$ and $d_{yz-xz}$ orbitals, have less than 7% character on the ligating nitrogens (Table 5). Note that the $\pi_1$ levels in **1** to lower binding energy are calculated to have even less character on the ligating nitrogens (<2%). Further, the appearance of low-energy band 2 in the MCD spectrum of **1** is consistent with the appreciable coordinating-N character in low-lying MO 49A. In contrast, the ligating nitrogens in the low-energy imidazole $\pi_2$-based MOs in plastocyanin, are calculated to have very little wave function character and, therefore, little contribution to the spectrum. Thus, the change from imidazole ligation to the Cu in plastocyanin to pyrazole ligation in **1** imparts clear changes to the spectral features that facilitates the assignment of the associated electronic transitions.

In summary, this study has investigated the effects of thiolate covalency in blue Cu-like sites. Relative to the prototypical blue Cu site in plastocyanin, the above data demonstrate that the stronger thiolate−Cu donor interaction in **1** quantitatively leads to an increase in the oscillator strength of the S p$\pi \rightarrow$ Cu CT transition, a stronger Cu−S bond, and a larger vibrational relaxation energy. Shifts to lower energy of the ligand field transitions point to a weaker ligand field in **1** consistent with its more tetrahedral site geometry. Differences in the electronic structure of imidazole and pyrazole also modify the spectral features associated with these ligands, which confirms that N(His) $\pi_1 \rightarrow$ Cu CT transitions contribute to the absorption intensity in plastocyanin in the ∼450 nm region. The electronic structure is also modulated by an increase in the $Z_{eff}$ of Cu upon changing from plastocyanin to **1**. This implies that the [$HB(pz')_3^-$] donor set in **1** is weaker than the $N(His)_2S(Met)$ donor set in plastocyanin, which is likely due to misdirection of the pyrazole donor orbitals due to the presence of the B−N bonds that restrain the Cu−N interaction in this facially coordinating, tridentate ligand system. This is consistent with the concept that changes in the $N(His)_2S(Met)$ donor set of the blue copper site can affect the covalency of the thiolate-Cu bond, which plays a key role in the electron-transfer properties of this site (i.e. low reorganization energy and covalent coupling into ET pathways).[81,82]

**Acknowledgment.** We thank Professor Thomas Brunold for the MathCAD script used for the time domain Raman analysis. Financial support for this research program came from the NSF (CHE-9980546 to E.I.S.) and the NIH (RR-01209 to K.O.H. and a postdoctoral fellowship GM-18812 to D.W.R.). K.F. is grateful for a grant (No. 11640555) for financial support of this work. SSRL operations are funded by the U.S. Department of Energy, Office of Basic Energy Sciences. The Structural Molecular Biology program at SSRL is supported by the National Institutes of Health, National Center for Research Resources, Biomedical Technology Program and by the Department of Energy, Office of Biological and Environmental Research.

**Supporting Information Available:** Table summarizing ADF calculation for plastocyanin; Figure showing the MCD spectrum of the $HB(pz')_3CuSC_6F_5$ complex; and input files for the calculations (PDF); an X-ray crystallographic file (CIF). This material is available free of charge via the Internet at http://pubs.acs.org.

JA001591W

(81) Randall, D. W.; Gamelin, D. R.; LaCroix, L. B.; Solomon, E. I. *J. Biol. Inorg. Chem.* **2000**, 5, 16−29.

(82) Solomon, E. I.; Randall, D. W.; Glaser, T. *Coord. Chem. Rev.* **2000**, *200−202*, 595−632.